SAND2020-5103C

Hyperspectral vegetation identification utilizing polynomial fitting for dimensionality reduction

John D. van der Laan[a], Brian J. Redman[a], Dylan Z. Anderson[a], R. Derek West[a], and David Yocky[a]

[a]Sandia National Laboratories, 1515 Eubank Blvd SE, Albuquerque, NM 87123, United States

ABSTRACT

Identification of vegetation species and type is important in many chemical, biological, radiological, nuclear, and explosive sensing applications. For instance, emergence of non-climax species in an area may be indicative of anthropogenic activity which can complement prompt signatures for underground nuclear explosion detection and localizing. To explore signatures of underground nuclear explosions, we collected high spatial resolution (10 cm) hyperspectral data from an unmanned aerial system at a legacy underground nuclear explosion test site and its surrounds. These data consist of 270 visible and near-infrared wavebands over 4.3 km^2 of high desert terrain along with high spatial resolution (2.5 cm) RGB context imagery. Previous work has shown that vegetation spectral derivative can be more indicative of species than the measured value of each band. However, applying a spectral derivative amplifies any noise in the spectrum and reduces the benefit of the derivative analysis. Fitting the spectra with a polynomial can provide the slope information (derivative) without amplifying noise. In this work, we simultaneously capture slope and curvature information and reduce the dimensionality of remotely sensed hyperspectral imaging data. This is performed by employing a 2$^{\text{nd}}$ order polynomial fit across spectral bands of interest. We then compare the classification accuracy of a support vector machine classifier fit to the polynomial dimensionality reduction technique and the same support vector machine fit to the same number of components from principle component analysis.

Keywords: hyperspectral imagery, underground nuclear explosions, unmanned aerial systems, vegetation, classification

1. INTRODUCTION

The detection, location, and characterization of suspected underground nuclear explosions (UNEs) are global security priorities that rely on integrated analyses of multiple data modalities for uncertainty reduction in event analysis. Current techniques rely on sensors recording prompt data, such as seismic or radionuclide monitoring networks.[1] While these prompt techniques can generally detect and locate suspected underground nuclear tests, the addition of non-prompt observables can add crucial event signatures. Non-prompt observables are critical for refining event location and characterization. Previously, we employed machine learning against collected hyperspectral imagery[2] to identify and map vegetation species in an area containing a legacy underground nuclear test site. We found that spatial species distributions clearly demarcate the site of interest but that limiting the classes of interest resulted in systematic errors.[3]

Vegetation around a suspected UNE provides a unique carrier for a number of potential signatures. Short and long term changes to the subsurface and water table may manifest as changes in vegetation health, water content, or growth. Vegetation can capture and hold on to surface and subsurface material for periods of days to decades.[4] The presence of non-native or earlier succession species[5] can reveal areas of anthropogenic activity long after specific artifacts or thermal signatures have decayed or been sanitized.

Numerous airborne and space based multi and hyperspectral imaging systems, such as Landsat, QuickBird, or AVIRIS,[6] have been applied to vegetation mapping applications. However, the long standoff distance for these systems results in course spatial resolution, ranging from meters to kilometers ground sample distance. Recently,

Further author information: (Send correspondence to B.J.R.)
B.J.R.: E-mail: bjredma@sandia.gov, Telephone: 1 505 284 6468

unmanned aerial systems (UAS) have emerged as a viable platform for optical remote sensing. UAS can fly much lower than traditional systems, thereby providing very high spatial resolution measurements. The high spatial resolution improves the ability to spatially resolve targets and reduces the need to use mixture models because there are fewer types of materials in each pixel. This high resolution along with the low cost of operation over small areas[7] makes UAS a prime platform for targeted vegetation mapping.

Remote vegetation mapping often make use of various vegetation indices.[8] While vegetation indices are proven tools for estimating properties such as biomass or ground coverage, they are severely lacking in discriminating power for discerning different vegetation species. Hyperspectral imaging (HSI) systems record higher spectral resolution which allows for differentiation of vegetation species.[9] HSI data has been used in previous work with statistical detection algorithms for geologic material characterization,[10] and with machine learning techniques for mapping vegetation species.[11]

Previous work shows that a vegetation spectral derivative can be more indicative of species than the measured value of each band.[12,13] However, applying a spectral derivative amplifies any noise in the spectrum and reduces the benefit of the derivative analysis. Fitting the spectra with a polynomial function can provide the slope information (derivative) without amplifying noise. Fitting the spectra also decreases the dimensionality of the data, decreasing processing and analysis time. In this work, we simultaneously capture slope and curvature information and reduce the dimensionality of remotely sensed HSI data. This is performed by employing a 2^{nd} order polynomial curve fits across spectral bands of interest. We then compare the classification accuracy of a support vector machine (SVM) classifier fit to the polynomial fit dimensionality reduction technique and the same SVM fit to the same number of components from principle component analysis (PCA).

This paper overviews HSI data collection and signature mapping in Section 2, the methods we employ for data reduction and vegetation mapping in Section 3, our results against legacy UNE test sites in Section 4, and concludes in Section 5.

2. BACKGROUND

Previously, we collected high spatial resolution (10 cm ground sample distance) hyperspectral imagery from a UAS at a legacy UNE test site and its surrounds.[2] These data consist of visible and near infrared (VNIR) wavebands over 4.3 km^2 of high desert terrain at the Nevada National Security Site (NNSS). The NNSS is a declared legacy nuclear explosion test range in southern Nevada, and is the site of over 800 UNE tests in a variety of geologies and emplacements (tunnels and boreholes).[14] Although the United States has placed a moratorium on UNE testing since 1992, the NNSS remains a laboratory for measuring and characterizing non-prompt and persistent signatures and observables. An overview of the HSI data collection is shown in Fig. 1. The HSI collection encompasses a large area with multiple UNE tests. For the quantitative analysis presented here we focus on the area located around the Barnwell site.

The area of interest is composed of Pinyon-juniper woodland, co-dominated by stands of evergreen junipers and pinyon pines and understory shrubs composed of rabbitbrush, and sagebrush. The scene is also punctuated by various species of wildflowers and grasses. Growth ring counting indicates that the climax community Pinyon-juniper stands are in excess of 50 years of age. The UNE tests in the AOI were conducted from 1987-1991, thus, much of the climax vegetation was established prior to, and lived during the tests. Prior to the tests, large areas around the boreholes were cleared of vegetation for equipment, vehicles, etc. This is reflected by secondary-stage succession vegetation communities that have not fully recovered to the climax stage even 30 years post test.

HSI sensors collect optical intensity measurements for hundreds of contiguous bands over a spectral range commonly including the VNIR wavebands. Illumination models are used to convert the intensity measurements of each pixel to reflectance profiles which are indicative of material type. In contrast to multispectral data, HSI bands are not optimized for a specific application or set of materials. This allows HSI to be used to identify a broader range of materials and applications. Additionally, HSI data allow for differentiation of materials that have similar spectral signatures such as healthy and diseased crops.[15]

Vegetation indices derived from the HSI data are used in this work as an initial processing step for mapping vegetation. These indices, typically differences or ratios between spectral bands, represent scores that are correlated with properties of the vegetation. The normalized difference vegetation index (NDVI) is the normalized

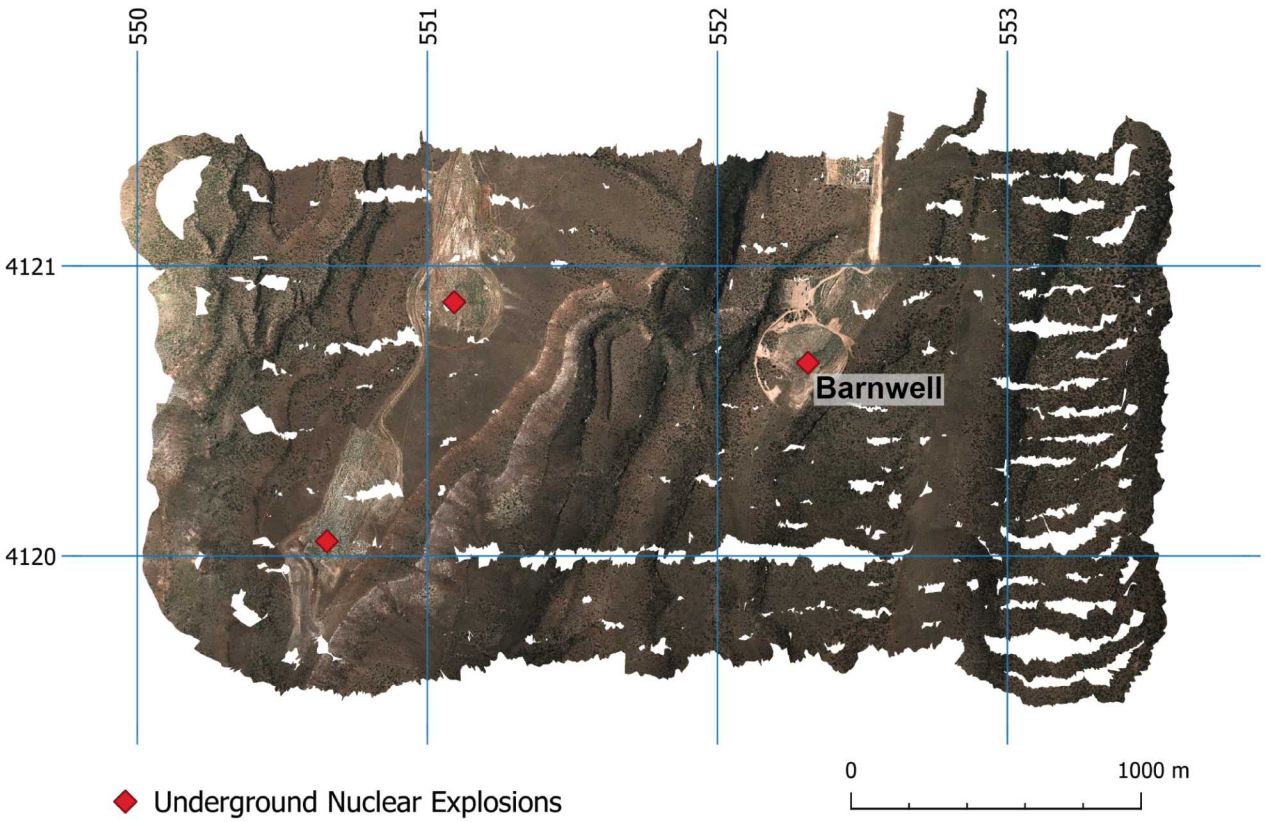

Figure 1: The pseudo-color overview of the visible and near infrared hyperspectral imagery. The grids represent 1 km UTM zone 11N coordinates, and the collection spans approximately 4.3 km^2. Three underground nuclear explosion sites are encompassed in the collection area along with diversion terrain and vegetation features. Quantitative analysis presented here is focused around the Barnwell site. Details of the collection can be found in Anderson et al.[2]

difference between reflectance in the red and near infrared wavelengths[16] and is perhaps the most ubiquitous index in practice. NDVI is a well established method for estimating the vegetation ground cover from multi-spectral satellite data because chlorophyll is highly absorbing in the red waveband and the internal structures of leaves makes vegetation highly reflective in the near infrared waveband.[17,18] For green vegetation, the NDVI usually ranges from 0.2 to 0.9.[19] Given the high spatial resolution of our collected HSI data, NDVI is a strong indicator of the presence of vegetation on a per-pixel basis.[19]

3. METHOD

Using the remotely sensed HSI data previously described, we employ two methods of dimensionality reduction. Dimensionality reduction is performed as a precursor step to classification of the vegetation in the scene using a SVM. Principle component analysis[20] (PCA) is a dimensionality reduction technique widely used with HSI data. PCA offers a number of benefits when working with large, high-dimensionality datasets such as HSI data. PCA is able to reduce the dimensionality of the large datasets while minimizing information loss.[21] We treat PCA as the current standard for dimensionality reduction of large datasets such as HSI data. In this work, we also explore polynomial curve fitting as an alternative dimensionality reduction technique for HSI data. Literature has shown that the derivative of spectra can be useful for identifying similar vegetation species.[12,13]

Prior to any dimensionality reduction, a number of steps are employed. The common workflow for all techniques is shown in Fig. 2. Much of this workflow is described in our previous publication.[3] Here we describe

any additions or modifications for this analysis but defer to the previous manuscript for detailed description of the rest of the workflow.

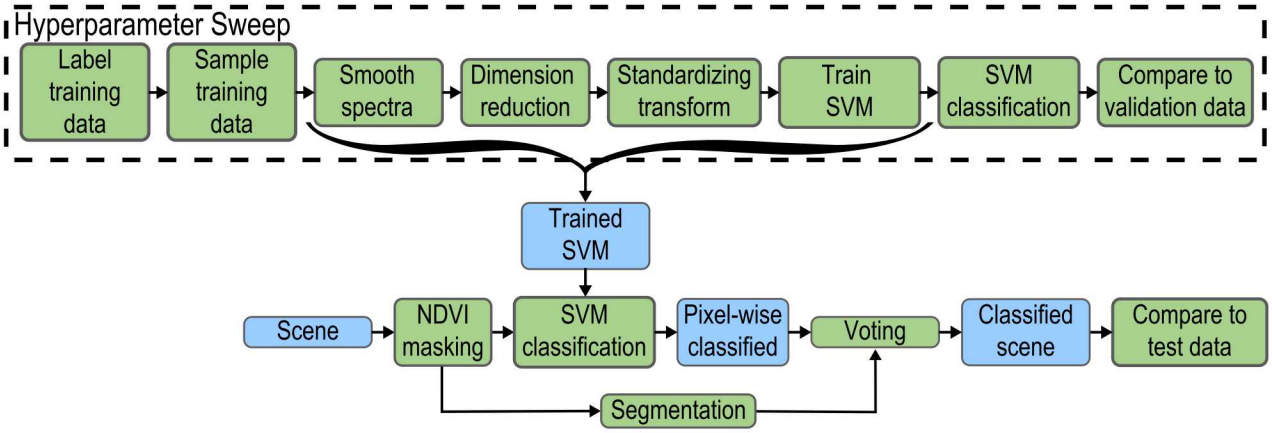

Figure 2: SVM common workflow for both dimensionality reduction techniques. The SVM was optimized using a hyper parameter sweep to maximize the classification accuracy of the validation data. The trained SVM was then applied to classify the vegetation across the scene for each technique.

Training data were selected from regions of the scene with predominately one vegetation species as shown in Fig. 3 (a). NDVI was performed over the entire scene and a threshold was used to select vegetation pixels only. The NDVI value of green vegetation usually ranges from 0.2 to 0.9,[19] thus a threshold value of 0.2 was chosen. Within each training data region a smaller subset was chosen and set aside for a validation dataset. The five vegetation classes of interest are described in Table 1. Classes 1 and 2 are the same, non-climax community species of shrub but class 1 consists of shrubs that regrew after a fire. Regions where either of these classes are predominant indicate that the vegetation species in the area were disturbed. Class 3 consists of climax community shrubs. Locations with these plants indicate that the vegetation in the region has not been recently disturbed. Class 4 consists of grasses which are not a strong indicator of whether the vegetation has been disturbed. In our previous analysis grasses were a common confuser for the other classes. Thus, we have chosen to include grass as a separate class to reduce false classifications. Class 5 consists of trees, both juniper and pinion, which are very strong indicators that the vegetation in a region has not been disturbed for a long time.

Table 1: SVM Vegetation Classes

Class	**Description**
1	the youngest shrubs that regrew after a fire
2	shrubs that regrew after the site was cleared, but were not burned
3	shrubs that had not been cleared and are part of the climax community of the region
4	grasses
5	pinyon and juniper trees

In addition to the training data, regions of the scene with predominantly one vegetation species were chosen for test data. These regions were selected to be disparate from the training data regions. The regions chosen for test data are shown in Fig. 3 (b).

Once training and test regions were determined, the spectrum for each pixel throughout the scene are convolved with a Gaussian profile for spectral smoothing. Each pixel's spectra originally consists of 274 values. The dimensionality reduction techniques were used to reduce the dimensionality by an order of magnitude.

The polynomial curve fitting was performed over seven specific spectral bands. The spectrum of each pixel was separated into the seven bands shown in Table 2. Chlorophyll present in vegetation offers specific spectral features than can be useful for classification. The seven specific spectral bands used for the polynomial fitting

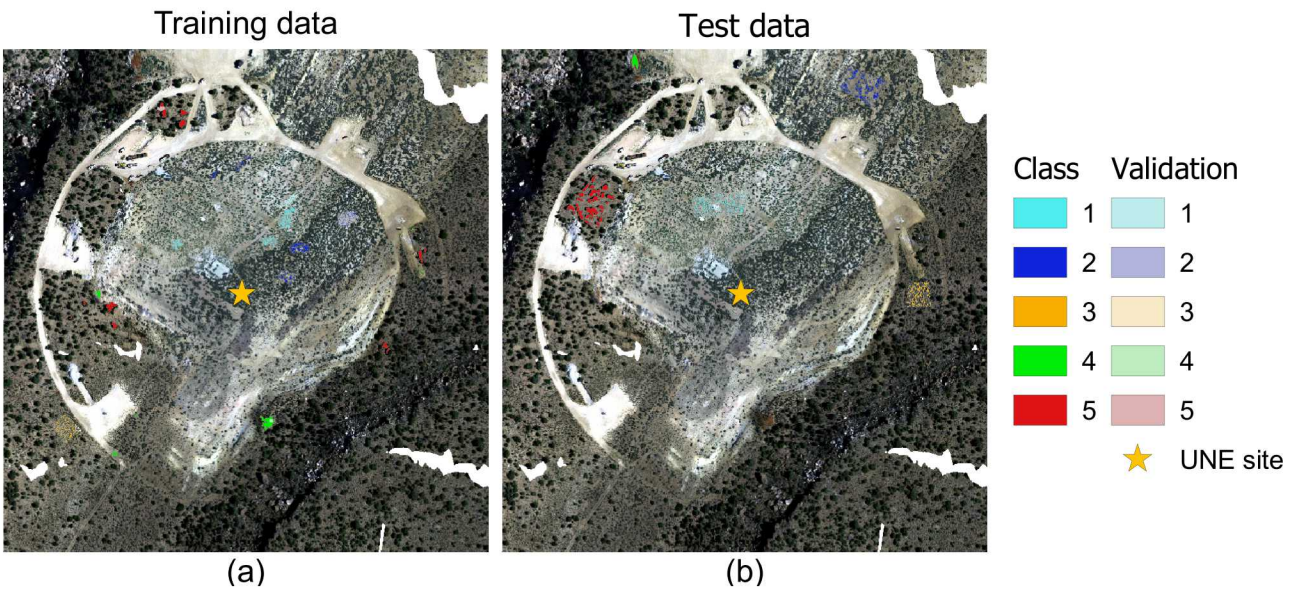

Figure 3: (a) Training data for the five vegetation classes was selected from pixels with NDVI greater than 0.2 in regions dominated by each type of vegetation. Small regions inside each train region were set aside for validation data. (b) Test regions were selected from different regions of the scene that were also dominated by the corresponding vegetation type.

were chosen to encompass spectral regions that are important for chlorophyll. The polynomial fitting technique allows subject matter experts to utilize expertise to choose targeted spectral bands to maintain as much useful data as possible during the data reduction process. Within each spectral band a 2^{nd} order polynomial curve is fit to the spectral data. The 0^{th}, 1^{st}, and 2^{nd} order values from each polynomial fit curve are then compiled for a total of twenty one feature values for each pixel.

Table 2: Spectral bands used for polynomial fitting dimensionality reduction.

Band	**Wavelength range**
1	440 nm $\rightarrow$ 452 nm
2	448 nm $\rightarrow$ 510 nm
3	518 nm $\rightarrow$ 586 nm
4	590 nm $\rightarrow$ 630 nm
5	632 nm $\rightarrow$ 692 nm
6	706 nm $\rightarrow$ 746 nm
7	772 nm $\rightarrow$ 890 nm

The second dimensionality reduction technique, PCA, was also performed on the original data. In order to compare the PCA results with the polynomial fitting technique, twenty one PCA components were chosen for the PCA data reduction technique. This ensures each technique has the same number of features for the SVM. For both techniques a standardizing transform was used to demean the features and force the standard deviation of each feature to one. Stardardized features are provided as input to the SVM. A hyperparameter sweep was performed for the SVM parameters. The SVM was optimized separately for each dimensionality reduction technique. The resulting optimized SVM parameters are shown in Table 3. Using these values and previously described methods the classification results in the following section were generated.

Table 3: Parameters[22] optimized by the hyperparameter sweep for each dimensionality reduction technique

Parameter	**PCA**	**Polynomial Fitting**
FWHM (nm)	7.37	5.77
Kernel	Radial Basis Function	Radial Basis Function
C	127.73	917.47
γ	6.07E-3	1.96E-3

4. RESULTS AND DISCUSSION

The trained SVM classifiers, using both PCA and polynomial fitting dimensionality reduction, were applied to a region around the Barnwell UNE site. All of the vegetation pixels, as selected with an NDVI mask greater than 0.2, were assigned into the five vegetation classes shown in Table 1. Classification results for both the PCA and polynomial fitting techniques is shown in Fig. 4 (a) and (b), respectively. Both techniques' classification results look very similar. In order to compare the two results Fig. 4 (c) shows the difference between the two techniques, revealing that differences are seemingly random and without specific structure. These different classifications for each technique are distributed throughout the entire scene.

Figure 4 (d) and (e) show results for classification using segmentation and voting. The addition of segmentation and voting allows the incorporation of spatial information into the classification process. For these segmentation results Felzenszwalb segmentation[23] was used. The Felzenszwalb segmentation extracted spatial features from the HSI image based on three spectral bands corresponding to red, green, and blue wavelengths. The resulting segments were variable in size in order to segment individual plants of different sizes. After the scene was segmented spatially the pixels within each segment were assigned to the class with the majority of pixels in the segment. This segmentation and voting method reduced the difference between the technique's results. The difference between each technique is shown in Fig. 4 (f). Similar to the original method, the different classifications for each technique are still distributed throughout the entire scene but are less prevalent.

Overall both dimensionality reduction techniques produce similar looking classification results with spatially distributed differences. The previously defined test regions of the scene, Fig. 3 (b), were used to quantitatively compare the classification accuracy of each technique. Quantitative analysis of the classification accuracy of the test regions shows both dimensionality reduction techniques provide similar performance. The addition of segmentation and voting also improved the classification accuracy for both techniques. Figure 5 shows confusion matrices for the test regions.

Quantitative analysis of the pixel-wise classifications, Fig. 5 (a) and (b), reveals substantial misclassification between the shrub classes (class 1, 2, and 3). This cross classification was expected to a degree. Vegetation classes 1 and 2 represent the same species, but their ages differ due to a recent fire. Vegetation class 3 is a different species than classes 1 and 2 but still represents a shrub. Classification performance of vegetation class 4 (grass) was very good for both pixel-wise methods. This class has a very distinct spectral signature compared to the other classes. There are some misclassifications of class 5, trees, with pixel-wise methods but significantly less than that present in the shrub classes.

The addition of segmentation and voting increased the classification accuracy for all vegetation classes. By assigning all segmented pixels to the majority class almost all the classification accuracies are above 90%. The only class with less than 95% accuracy is class 2, shrubs that regrew after the site was cleared but were not burned. Vegetation class 2 is still misidentified as class 1 even with segmentation and voting. This classification error for class 2 may be due to younger shrubs, class 1, present in the test data regions for class 2. Vegetation class 2 test regions were chosen where mature shrubs dominated the area. Even with careful visual inspection it is not always clear where class 1 shrubs may have proliferated within the class 2 regions. Both dimensionality reduction techniques exhibit the same misclassification percentage of class 2 as class 1. This fact supports the hypothesis that the misclassification error is likely due to the presence of younger shrubs in the class 2 test regions.

Overall, the classification accuracies of both dimensionality reduction techniques are nearly equivalent with both pixel-wise or segmentation and voting methods. The use of segmentation and voting decreases the misclassification found in the pixel-wise method for classes 1 to 3 and class 5. These results clearly show that segmentation

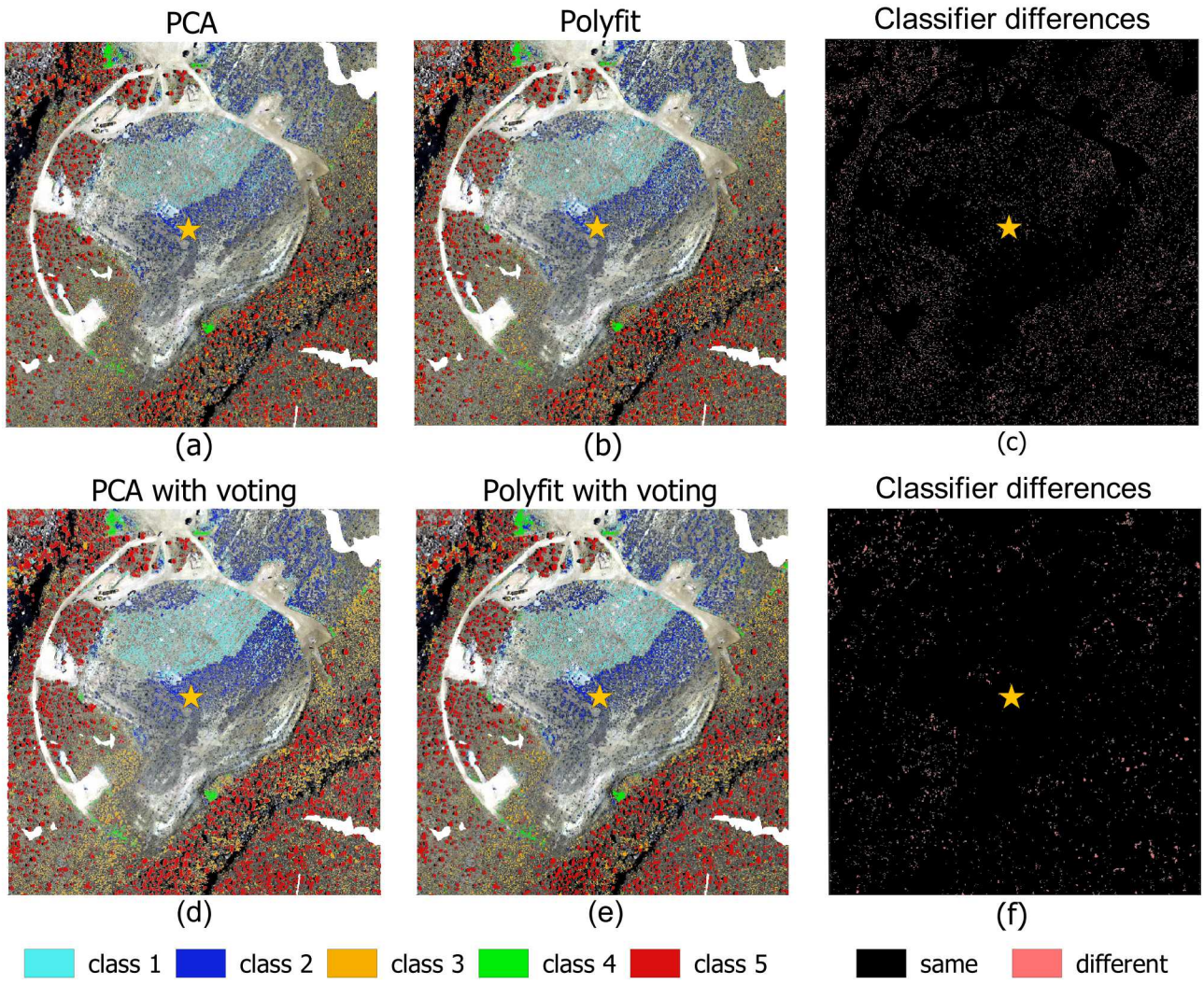

Figure 4: (a) SVM classification results using PCA dimensionality reduction. (b) SVM classification results using polynomial fitting dimensionality reduction. (c) Differences between the classification results for each technique. Results show in (d-f) use segmentation and voting to incorporate spatial information with the classification. The star in each image indicates the location of the Barnwell UNE site.

and voting results in very high classification accuracy. The addition of segmentation and voting also removes nearly all differences between the two dimensionality reduction techniques performance. Classification accuracy differences between the two dimensionality reduction techniques with segmentation and voting is less than 2%.

With the information learned from testing the trained SVM on the smaller Barnwell UNE site region, we expand our classification area to encompass the entire HSI collection region. The results from this effort with PCA and polynomial fitting are shown in Fig. 6 (a) and (b), respectively. Our goal in this is to identify the locations of the surrounding UNE sites by position and density of the various vegetation species/classes. Regions where vegetation classes 3 and 5 are absent and classes 1 and 2 dominate are highly indicative of where the ground was cleared for the UNE sites. These regions can clearly be observed as aqua and blue regions for both dimensionality reduction techniques in Fig. 6. Both PCA and polynomial fitting techniques produce results that highlight the location of the three UNE sites (star locations) throughout the HSI collection region. The differences between the dimensionality reduction techniques do not produce a systematic difference across the image. These results indicate that vegetation species can indicate areas of anthropomorphic activity such as ground clearing.

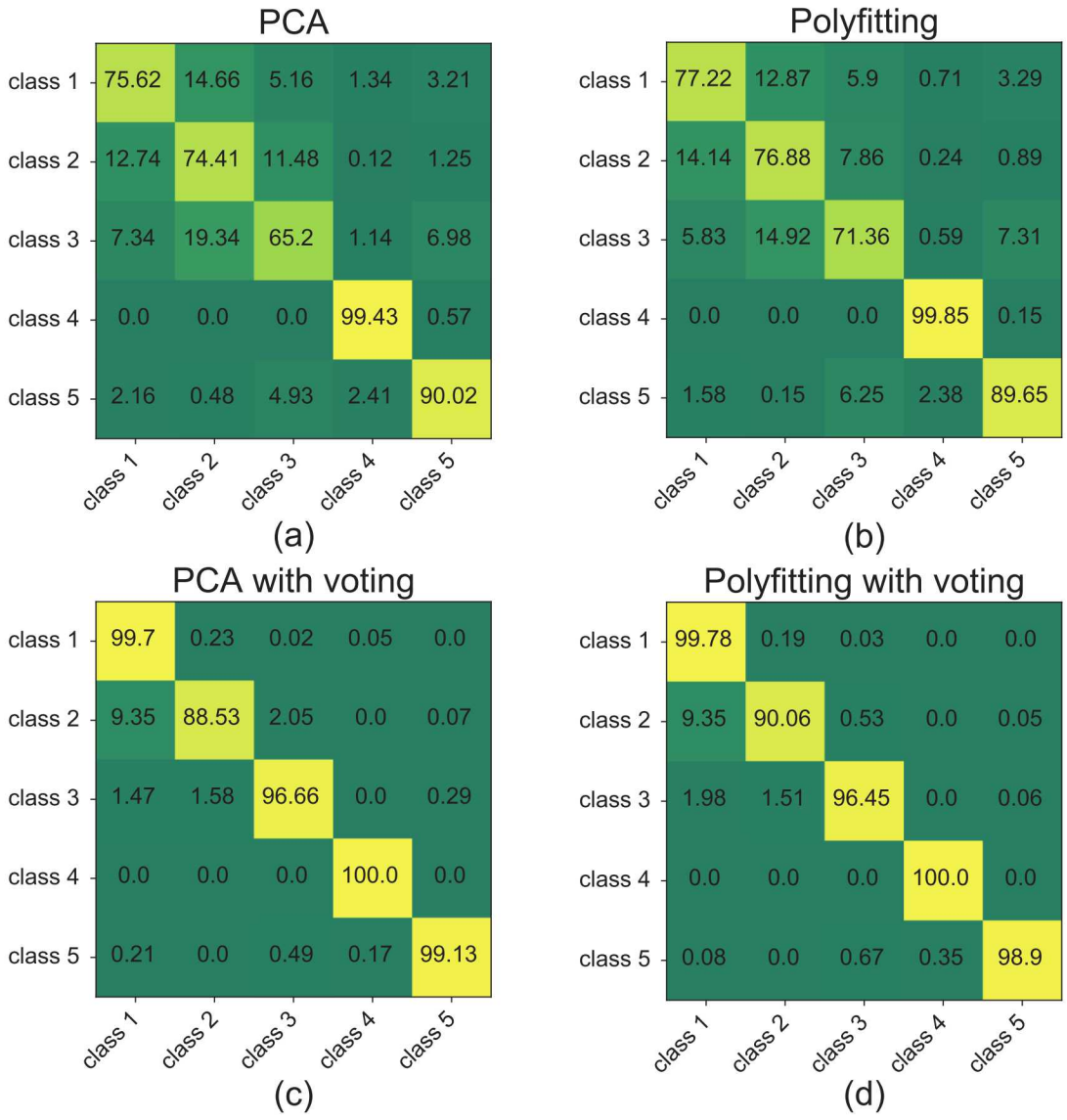

Figure 5: Confusion matrices of the SVM classifier: (a) pixel-wise accuracy using PCA for dimensionality reduction, (b) pixel-wise accuracy using polynomial fitting for dimensionality reduction, (c) accuracy with segmentation and voting using PCA for dimensionality reduction, and (d) accuracy with segmentation and voting using polynomial fitting for dimensionality reduction.

These types of vegetation signatures can be readily observed from remote locations and be added to the collection of signatures and observables used to locate and characterize underground nuclear testing locations.

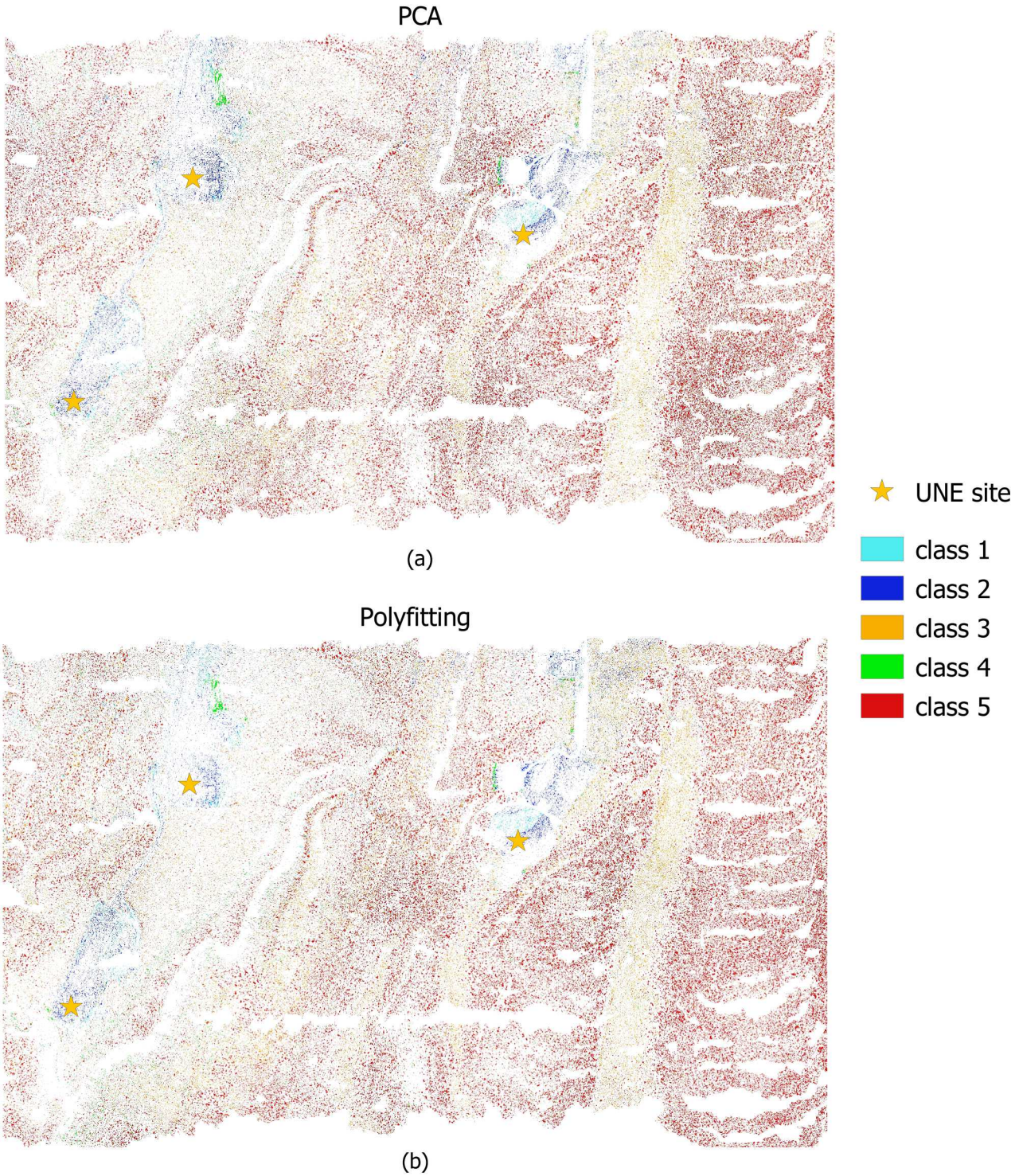

Figure 6: Optimized trained SVMs were used to classify an area containing three UNE sites. (a) Classification results using PCA dimensionality reduction. (b) Classification results using polynomial fitting dimensionality reduction. Both techniques produce satisfactory results for the larger scene.

5. CONCLUSIONS

Throughout this manuscript we have tested the classification accuracy and performance of two different dimensionality reduction techniques for HSI data. The two techniques we pursued were a traditional PCA approach and a unique polynomial fitting approach that can leverage subject matter expert input. Our hypothesis was that the additional focused choice of spectral bands by the expert had potential to outperform PCA. The results described here show that using either polynomial fitting or PCA for dimensionality reduction of the HSI vegetation data, classified by an SVM, resulted in nearly equivalent classification accuracies. For most use cases, PCA offers a much easier technique for dimensionality reduction. PCA is widely accepted, has been heavily optimized, and does not require a user to have *a priori* expert knowledge of useful spectral features. If the user does have *a priori* knowledge of spectral bands of interest then the use of the polynomial fitting technique could emphasize those bands and spectral properties.

Regardless of the dimensionality reduction approach chosen, incorporating spatial information through segmentation and voting has a stronger impact on the classification accuracy than the data reduction method. With the addition of segmentation and voting, both approaches yielded very high classification accuracy, typically above 95%. The results presented here demonstrate that an SVM trained on dimensionality reduced data can differentiate the type of species and those species maturity levels using remotely sensed VNIR HSI data. For any classification task using these methods care must be taken when defining test regions, as was shown for vegetation classes 1 and 2. Lastly, we have shown that classification of vegetation over large areas can detection locations of non-climax community vegetation growth. These areas are a strong indicator of possible activity related to UNE site development and testing, as well as other anthropomorphic development.

6. ACKNOWLEDGMENTS

The authors would like to thank the National Nuclear Security Administration, Defense Nuclear Nonproliferation Research and Development, for sponsoring this work. We would also like to thank the Underground Nuclear Explosion Signatures Experiment team, a multi-institutional and interdisciplinary group of scientists and engineers, for its technical contributions and support at the NNSS.

Sandia National Laboratories is a multimission laboratory managed and operated by National Technology & Engineering Solutions of Sandia, LLC, a wholly owned subsidiary of Honeywell International Inc., for the U.S. Department of Energy's National Nuclear Security Administration under contract DE-NA0003525.

This paper describes objective technical results and analysis. Any subjective views or opinions that might be expressed in the paper do not necessarily represent the views of the U.S. Department of Energy or the United States Government.

REFERENCES

[1] Hoffmann, W., Kebeasy, R., and Firbas, P., "Introduction to the verification regime of the comprehensive nuclear-test-ban treaty," *Physics of the Earth and Planetary Interiors* **113**(1-4), 5–9 (1999).

[2] Anderson, D., Craven, J. M., Dzur, R., Briggs, T., Lee, D. J., Miller, E., Schultz-Fellenz, E., and Vigil, S., "Using unmanned aerial systems to collect hyperspectral imagery and digital elevation models at a legacy underground nuclear explosion test site," *Proc.SPIE* **10656** (2018).

[3] Redman, B. J., van der Laan, J. D., Anderson, D. Z., Craven, J. M., Miller, E. D., Collins, A. D., Swanson, E. M., and Schultz-Fellenz, E. S., "Hyperspectral vegetation identification at a legacy underground nuclear explosion test site," in [*Chemical, Biological, Radiological, Nuclear, and Explosives (CBRNE) Sensing XX*], Guicheteau, J. A. and Howle, C. R., eds., **11010**, 145 – 154, International Society for Optics and Photonics, SPIE (2019).

[4] Howard, B. J., Semioschkina, N., Voigt, G., Mukusheva, M., and Clifford, J., "Radiostrontium contamination of soil and vegetation within the semipalatinsk test site," *Radiation and Environmental Biophysics* **43**, 285–292 (Dec 2004).

[5] Horn, H. S., "The ecology of secondary succession," *Annual Review of Ecology and Systematics* **5**(1), 25–37 (1974).

[6] Xie, Y., Sha, Z., and Yu, M., "Remote sensing imagery in vegetation mapping: a review," *Journal of Plant Ecology* **1**(1), 9–23 (2008).

[7] Matese, A., Toscano, P., Di Gennaro, S. F., Genesio, L., Vaccari, F. P., Primicerio, J., Belli, C., Zaldei, A., Bianconi, R., and Gioli, B., "Intercomparison of uav, aircraft and satellite remote sensing platforms for precision viticulture," *Remote Sensing* **7**(3), 2971–2990 (2015).

[8] Bannari, A., Morin, D., Bonn, F., and Huete, A. R., "A review of vegetation indices," *Remote Sensing Reviews* **13**(1-2), 95–120 (1995).

[9] Cochrane, M. A., "Using vegetation reflectance variability for species level classification of hyperspectral data," *International Journal of Remote Sensing* **21**(10), 2075–2087 (2000).

[10] Asadzadeh, S. and de Souza Filho, C. R., "A review on spectral processing methods for geological remote sensing," *International Journal of Applied Earth Observation and Geoinformation* **47**, 69 – 90 (2016).

[11] Burai, P., Deák, B., Valkó, O., and Tomor, T., "Classification of herbaceous vegetation using airborne hyperspectral imagery," *Remote Sensing* **7**(2), 2046–2066 (2015).

[12] Myneni, R. B., Hall, F. G., Sellers, P. J., and Marshak, A. L., "The interpretation of spectral vegetation indexes," *IEEE Transactions on Geoscience and Remote Sensing* **33**(2), 481–486 (1995).

[13] Thorp, K., Tian, L., Yao, H., and Tang, L., "Narrow-band and derivative-based vegetation indices for hyperspectral data," *Transactions of the American Society of Agricultural Engineers* **47**(1), 291–299 (2004). cited By 20.

[14] U.S. Department of Energy, National Nuclear Security Administration Nevada Field Office, "United States Nuclear Tests, July 1945 through September 1992," *DOE/NV—209-REV 16* , 186 (2015).

[15] Mahlein, A.-K., Oerke, E.-C., Steiner, U., and Dehne, H.-W., "Recent advances in sensing plant diseases for precision crop protection," *European Journal of Plant Pathology* **133**, 197–209 (May 2012).

[16] Jackson, R. D. and Huete, A. R., "Interpreting vegetation indices," *Preventive Veterinary Medicine* **11**(3), 185 – 200 (1991).

[17] Huete, A., Didan, K., Miura, T., Rodriguez, E., Gao, X., and Ferreira, L., "Overview of the radiometric and biophysical performance of the modis vegetation indices," *Remote Sensing of Environment* **83**(1), 195 – 213 (2002). The Moderate Resolution Imaging Spectroradiometer (MODIS): a new generation of Land Surface Monitoring.

[18] Knipling, E. B., "Physical and physiological basis for the reflectance of visible and near-infrared radiation from vegetation," *Remote Sensing of Environment* **1**(3), 155 – 159 (1970).

[19] Candiago, S., Remondino, F., De Giglio, M., Dubbini, M., and Gattelli, M., "Evaluating multispectral images and vegetation indices for precision farming applications from uav images," *Remote Sensing* **7**(4), 4026–4047 (2015).

[20] Rodarmel, C. and Shan, J., "Principal component analysis for hyperspectral image classification," *Surveying and Land Information Science* **62**(2), 115–122 (2002).

[21] Jolliffe, I. and Cadima, J., "Principal component analysis: a review and recent developments," *Phil. Trans. R. Soc. A.* **374**(20150202) (2016).

[22] scikit-learn developers (BSD License), *RBF SVM parameters* (2019 (accessed May 11, 2020)). https://scikit-learn.org/stable/auto_examples/svm/plot_rbf_parameters.html.

[23] Felzenszwalb, P. F. and Huttenlocher, D. P., "Efficient graph-based image segmentation," *International Journal of Computer Vision* **59**, 167–181 (Sep 2004).